Geoderma Regional 34 (2023) e00690

Contents lists available at ScienceDirect

Geoderma Regional

journal homepage: www.elsevier.com/locate/geodrs

Macro-scale spatial modeling reveals the role of soil organic matter quality in CO_2 emissions

Renan Francisco Rimoldi Tavanti [a,*], Marcos Lado Liñares [a], Matheus Bortolanza Soares [b], Rodrigo Gonçalves Trevisan [c], Tauan Rimoldi Tavanti [d], Onã da Silva Freddi [e], Rafael Montanari [f], Antonio Paz González [a]

[a] Centro de Investigaciones Científicas Avanzadas, Faculty of Sciences, University of A Coruña, Coruña 15071, Spain
[b] Department of Soil Science, Luiz de Queiroz College of Agriculture, University of São Paulo, Piraciaba 13418900, Brazil
[c] Department of Crop Sciences, University of Illinois at Urbana-Champaign, Urbana 61820, USA
[d] Department of Crop Science and Social Economy, São Paulo State University "Julio de Mesquita Filho", Ilha Solteira 15385-000, Brazil
[e] Institute of Agricultural and Environmental Sciences, Federal University of Mato Grosso, Sinop 78557267, Brazil
[f] Department of Plant Health, Rural Engineering and Soils, São Paulo State University "Julio de Mesquita Filho", Ilha Solteira 15385-000, Brazil

ARTICLE INFO

Keywords:
Organic carbon
Land use change
Sustainable soil management
Greenhouse gas emissions
Infrared spectroscopy

ABSTRACT

Carbon dioxide (CO_2) emissions from agricultural soils result from the interaction of various factors that regulate the quantity and quality of organic material. Our objective was to assess changes in soil CO_2 fluxes following the renewal of degraded pastures using FTIR spectroscopy and a machine learning approach. Additionally, we aimed to understand the spatial distribution of organic compounds obtained from FTIR spectra bands and their correlations with soil attributes. The study was conducted in Selvíria, Mato Grosso do Sul, Brazil, in two areas dedicated to extensive beef cattle farming. Geostatistical grids were established in the study areas to evaluate CO_2 emissions, and soil sampling was performed for FTIR spectral analysis and other soil attributes. The semi-quantitative analysis of the CH vibrational region involved spectral deconvolution guided by the positions of the peaks obtained from the second derivative and Gaussian curve fitting. Our results indicate that the relative abundance of compounds related to peaks at 2853 cm^{-1} and 2923 cm^{-1} showed linear and spatial correlations with CO_2 emissions. Pasture renewal, followed by sorghum cultivation intercropped with *Urochloa brizantha*, resulted in increased soil pH up to 5.6 and reduced concentrations of compounds related to the aliphatic CH band. This management practice also led to a decrease in CO_2 emissions to a range of 0.94 to 0.97 μmol m^{-2} s^{-1}. The CH_2 index, calculated as the ratio of peaks at 2853 cm^{-1} and 2923 cm^{-1}, exhibited similar changes and could serve as an indicator of soil organic matter loss and CO_2 emissions in these systems. Our findings suggest that FTIR organic compounds are spatially dependent and coupled with a machine learning approach is sensitive to distinguish chemical changes in soil organic groups and predict soil CO_2 emissions.

1. Introduction

In the last century, the global demand for food has been linked to population growth and an increase in per capita income (Rask and Rask, 2011). The preferred approach to meeting this demand has been through agricultural extensification processes, primarily focused on grain and beef production (Tilman et al., 2011; Ray et al., 2013). However, the expansion of agricultural areas has had negative impacts on various natural ecosystems (Tilman et al., 2002; Lapola et al., 2014), resulting in the loss of forests in Africa and Asia, with over 75% of the lost forest area converted to agricultural land. In South America, nearly three-quarters of deforestation is due to livestock (FAO, 2020).

In Brazil, extensive livestock systems still dominate agricultural activities. Livestock feed heavily relies on pastures, with limited supplementation through mineral salts. One of the main characteristics of these systems is the lack of investment in chemical and physical soil preparation to enhance pasture productivity, leading to widespread degradation (Tavanti et al., 2020a). Extensive agricultural production systems in Brazil generally exhibit gradients of fertility and acidity (Vieira et al., 2008), surface compaction (de Assis Valadão et al., 2015), and low

* Corresponding author.
E-mail address: renan.tavanti@col.udc.es (R.F.R. Tavanti).

https://doi.org/10.1016/j.geodrs.2023.e00690
Received 14 March 2023; Received in revised form 25 July 2023; Accepted 27 July 2023
Available online 28 July 2023
2352-0094/© 2023 The Authors. Published by Elsevier B.V. This is an open access article under the CC BY license (http://creativecommons.org/licenses/by/4.0/).

carbon stocks (C) in the topsoil (Almeida et al., 2015), thus characterizing these areas as extractive and degraded systems.

In addition to soil characteristics that are unfavorable for animal productivity, pastures in various stages of degradation can contribute to increased loss of soil organic matter (SOM) due to reduced quality and quantity of organic materials added to the soil. This combination of low productivity and SOM loss leads to higher greenhouse gas emissions per kilogram of meat or milk produced (IPCC, 2017), resulting in negative public perception of livestock activities. Therefore, the adoption of sustainable soil land management (SLM) is necessary to maintain land cover, ensure animal production, and consider the quantity and quality of supplied organic matter (Sanz et al., 2017). Agricultural practices such as periodic correction of soil acidity, appropriate fertilization, optimal stocking capacity, and crop rotation are viable alternatives for rehabilitating degraded pastures, which can help reduce greenhouse gas emissions and maintain or increase meat productivity in the country.

During pasture renovation operations, soil preparation leads to increased CO_2 emission rates from the soil to the atmosphere. This is due to the solubilization of carbonates (from limestone) and the breakdown of soil aggregates. A portion of the carbon (C) occluded in the aggregates becomes susceptible to mineralization as it is exposed to microbial activity, facilitated by increased oxygenation and soil temperature (Schwartz et al., 2010; Silva et al., 2014). However, there is a reduction in labile fractions of SOM in the short term, accompanied by a decline in basal microbial activity, leading to the establishment of a new dynamic equilibrium (Six et al., 2006). This results in medium- and long-term reductions in CO_2 emissions and an increase in soil carbon stocks. As this is a relatively recent occurrence, there are limited studies in tropical areas that characterize the process of CO_2 emissions and assess changes in SOM quality following pasture renovation with crop rotations.

The quantity and quality of SOM are important indicators in soil fertility management (Paul, 2016) and can guide future strategies for implementing SLM practices. Traditionally, changes in the chemical composition of SOM have been evaluated using wet chemical fractionation, commonly known as the Van Soest method (Van Soest et al., 1991). This method provides accurate characterization of residue composition in different lability fractions and is considered a reference in studies of residue decomposition (Chen et al., 2010; Soong et al., 2014). However, it does not offer additional information about the structures of organic compounds and generates chemical waste after the analysis procedure (e.g., potassium dichromate). Due to these limitations, studies based on Fourier-transform infrared spectroscopy (FTIR) have successfully distinguished chemical components in organic materials during the decomposition process. FTIR can identify the presence of Si—O, CO, CN, C—H, and C—O bonds in polysaccharides, as well as C═C and COO- bonds in aromatic compounds (Duboc et al., 2012; McKee et al., 2016). This technique is increasingly used in soil science due to its versatility, rapid measurement speed, relatively low cost, and sensitivity to mineral and organic bonds that constitute SOM (Nocita et al., 2015; Parikh et al., 2014).

The combination of FTIR spectroscopy, physical fractionation of SOM, and a multivariate statistical approach (dimensionality reduction and machine learning) can provide valuable insights into the quality of agricultural systems. Understanding the specific SOM compounds that modulate CO_2 emissions from the soil, particularly in the context of pasture renovation operations, is still in its early stages. By employing various machine learning techniques such as Multiple Linear Regression, Partial Least Squares Regression, Artificial Neural Networks, or Random Forest (RF), it becomes feasible to predict soil attributes and gain insights into the significance of variables within the model. Among these methods, the RF model, which extends tree-based classification and regression algorithms, has been widely recognized as the most effective approach for classifying and quantifying soil properties (Rossel et al., 2006; Goydaragh et al., 2021; Rial et al., 2016).

In this context, we hypothesize that organic compounds obtained through FTIR spectroscopy can be utilized to map soil CO_2 emissions in areas undergoing pasture renewal, as well as other spatially dependent attributes such as pH and carbon stocks. Our objective was to evaluate changes in CO_2 fluxes by employing FTIR spectroscopy and a machine learning model as a framework after the renewal of degraded pastures. Additionally, we aimed to understand the spatial distribution of organic compounds obtained from bands in FTIR spectra and their correlations with soil attributes.

2. Material and methods

2.1. Study location and treatments assignment

The experiment was conducted in Selvíria county, Mato Grosso do Sul, Brazil, specifically at coordinates 20° 21′ S, 51° 24′ W, and an altitude of 357 m. The climate in this region can be classified as tropical and humid, characterized by a dry period in winter and a rainy period in summer (according to the Köppen's classification, it falls under the Aw category). The average annual temperature is 25 °C, and the annual precipitation reaches 1330 mm. The local soil was classified as loamy sand Oxisol, according to Soil Taxonomy (Soil Survey Staff, 2014), with a clay content of 130 g kg^{-1}, silt of 60 g kg^{-1}, and sand of 810 g kg^{-1}, as determined by the pipette method (Embrapa, 2017). The chemical characteristics of the soil before the beginning of the experiment were: organic matter content of 17.0 g kg^{-1}, pH in $CaCl_2$ of 4.9, exchangeable P of 5.8 mg kg^{-1}, exchangeable K of 0.6 $mmol_c$ kg^{-1}, exchangeable Ca of 9.4 $mmol_c$ kg^{-1}, exchangeable Mg 10.5 $mmol_c$ kg^{-1}, exchangeable Al 0.9 $mmol_c$ kg^{-1}, cation exchange capacity at pH 7.0 (CEC) 40.5 $mmol_c$ kg^{-1} and base saturation 50.1%, determined according to Van Raij et al. (2001).

The experiment was conducted on a farm, intended for the exploitation of beef cattle, with the planting and grazing of *Urochloa brizantha* cv. Marandu. Both the managed and unmanaged area have received over the years 2002, 2008, and 2013, corrections for soil fertility and acidity, with 1.5 t ha^{-1} of lime (25% CaO and 16% MgO), 31 kg ha^{-1} of urea (45% N), 123 kg ha^{-1} of triple superphosphate (40% P_2O_5 and 10% Ca), and 47 kg ha^{-1} of potassium chloride (60% K_2O).

The managed area received pasture management in 2017 in order to cultivate forage sorghum (*Sorghum bicolor* L. Moench) for silage production in the rainy season. The pasture was removed using a heavy disk harrow and, subsequently, 1,0 t ha^{-1} of lime was applied to raise the base saturation to 60%. Afterward, limestone was incorporated with an intermediate disk harrow and the ground was leveled with a light disk harrow. Fertilization was carried out during planting with 45 kg ha^{-1} of urea (45% N), 175 kg ha^{-1} of triple superphosphate (40% P_2O_5 and 10% Ca), and 67 kg ha^{-1} of potassium chloride (60% K_2O), and sorghum were seeded together with *U. brizantha*, both in broadcast forms. The planned population density of sorghum plants was 150,000 plants ha^{-1}. After these operations, the soil did not receive any other type of chemical or physical management. The dates and an illustrative scheme of the operations that made up the pasture renewal process are shown in Fig. 1.

In this context, two plots of the farm, possessing similar soil and topography characteristics, were selected as experimental areas for soil attribute mapping. Consequently, the treatments were characterized as follows:

Experimental Area 1 (Managed grassland): The first area underwent pasture renovation, employing the aforementioned procedures, to facilitate the cultivation of sorghum and *U. brizantha* for silage production. This allowed for cost amortization related to soil fertility and acidity corrections (Fig. 1). The animal stocking rate was maintained at 3 AU ha^{-1} $year^{-1}$. Throughout the sorghum production period (100 days), the animals were not allowed to graze. Subsequently, after the sorghum harvest, the area was made available for grazing.

Experimental Area 2 (Unmanaged grassland): The second experimental area retained its management system unchanged since 2013 (Fig. 1). The animal stocking rate remained at 3 AU ha^{-1} $year^{-1}$.

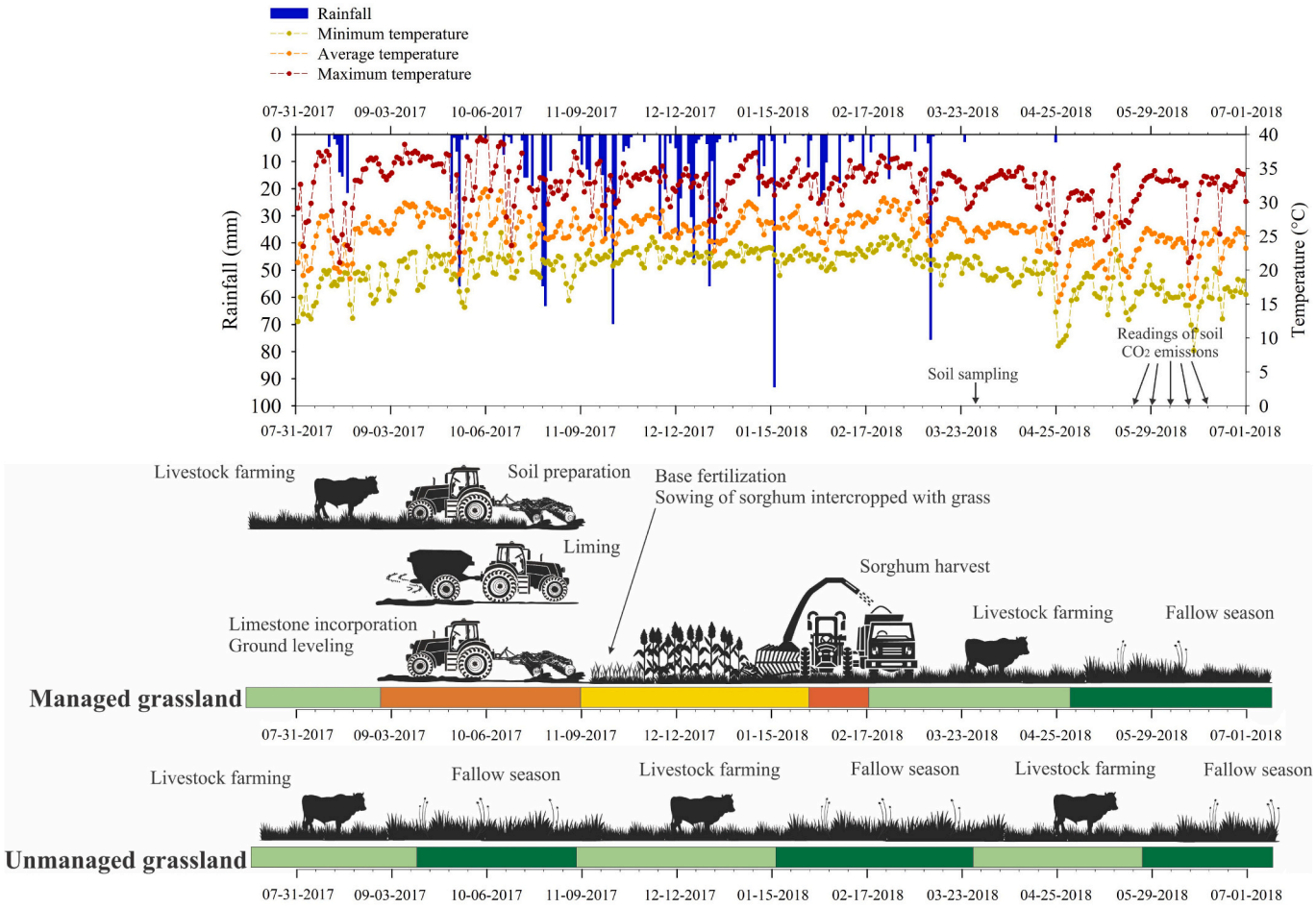

Fig. 1. Daily minimum, average, and maximum precipitation, and temperatures during the period of conducting the experiment in an Oxisol. The illustrations below the graph correspond to the management histories of the areas as well as their respective realization dates, as shown in the X-axis of the graph.

2.2. Sampling scheme

Georeferenced sampling grids were installed, with one grid implemented in each experimental area. The dimensions of the grids were equivalent to 1.4 and 2.7 ha, encompassing 65 and 70 points respectively (Fig. 2). To investigate the spatial dependence of soil attributes during the geostatistical analysis, certain locations were marked with points positioned in an orderly and sequential manner, spaced every five meters. The remaining points were randomly allocated to ensure representation across the entire perimeter of the area.

2.3. Sample preparation for FTIR spectroscopic measurements

Disturbed soil samples were collected from the 0.00–0.15 m layer using a Dutch-type auger. These samples were air-dried and subsequently crushed to pass through a 2 mm sieve. To ensure constant weight, the soil was then oven-dried at 60 °C for 15 h. For obtaining absorption spectra, the soil samples were diluted with KBr in a ratio of 1:300. Maceration using an agate mortar was employed to mix the soil samples with KBr. To ensure a flat surface, soil-KBr pellets were prepared using the Specac® GS01152 Palletizer, applying a fixed weight of 2 tons for two minutes. Following the pressing, the pallets were stored in a glass container with silica to prevent moisture absorption before FTIR readings.

The FTIR absorbance spectra were measured using a Nicolet™ iS10 FTIR spectrometer equipped with a KBr/Ge mid-infrared beam splitter. The instrument featured a Deuterated TriGlycine Sulfate (DTGS) detector and was accompanied by Smart Omni Transmission™ accessories. The measurements were conducted in a controlled environment with an ambient temperature of 25 ± 1 °C and humidity levels below 75%. Calibration and quality control of the analysis involved determining the background spectrum with pure KBr and performing polarization, noise, and atmospheric corrections for water vapor and CO_2. The FTIR spectrum was acquired over the range of 4000 to 400 cm^{-1} at a resolution of 8 cm^{-1} and a scanner velocity of 7.5 kHz. Each sample's average spectrum was derived from 64 scans, with the exclusion of the first and last points due to their consistent zero amplitude. Consequently, a total of 3734 points per soil sample were considered for further analysis.

2.4. Spectral data processing

Extended multiplicative signal correction (EMSC) (Griffiths and De Haseth, 2007) was employed for corrections and baseline spectra adjustments. EMSC applies a model-based approach for background correction and spectrum normalization. It effectively handles variations in scaling, polynomial baselines, and interferents. In the traditional EMSC preprocessing framework, the spectra were scaled using a predetermined reference spectrum, and irrelevant polynomial trends were subtracted from the data. The EMSC package in the R environment was utilized for this purpose, with a second-degree polynomial function defined as the model background (Fig. 3A). The resulting FTIR spectra of the soil samples are presented in Fig. 3B.

The chemical composition of SOM was evaluated by analyzing the peak intensity corresponding to the 2955–2830 cm^{-1} band (Band A), which corresponds to saturated aliphatic (alkane/alkyl) group frequencies, including symmetric and asymmetric stretching vibrations of

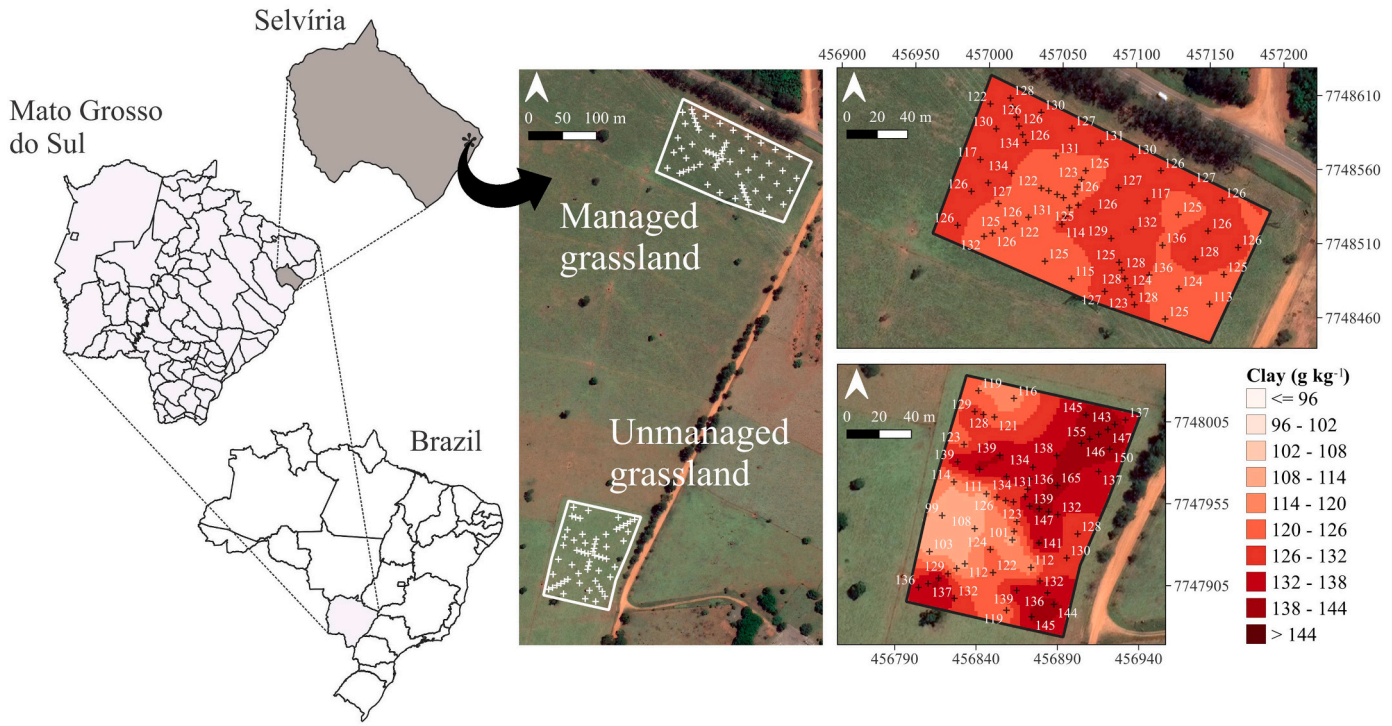

Fig. 2. Study location and representation of sampling grids with respective georeferenced points (+) in managed grassland (renewed) and unmanaged grassland areas. EPSG: 32722 – WGS 84 / UTM zone 22 S.

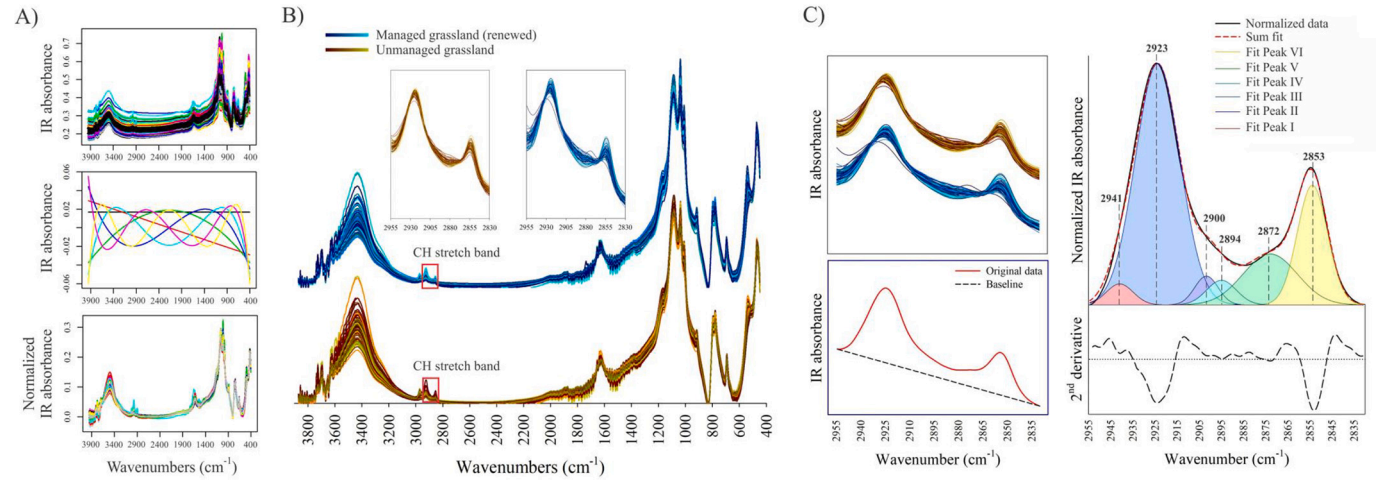

Fig. 3. FTIR spectral data processing of bulk soil samples from managed (renewed) and unmanaged grasslands. (A) Raw spectra; EMSC polynomials from 1 to 6° and; normalized spectra. (B) Normalized spectra separated by soil management system – in evidence the CH stretch band. (C) Baseline corrections of the C—H vibrational region; spectral deconvolution guided by the position of the peaks obtained in the second derivative and; Gaussian curve fitting to semi-quantitative estimate of the peaks obtained by integrating the AUC.

CH bonds (Fig. 3C). Band A was selected due to its representation of functional groups with high lability (aliphatic structures) in SOM. The choice of bands below 3000 cm^{-1} aimed to eliminate potential effects of O—H vibrations from water molecules. Deconvolution of the Band A peaks was performed by adjusting Gaussian curves based on the second derivative of the band. The minimum peaks of the second derivative were utilized to define the peaks in the normalized spectrum. Nonlinear least-squares fitting was applied to fit Gaussian curves. The semi-quantitative estimate of the peaks was obtained by integrating the area under the Gaussian curve (AUC) using the trapezium method. The identification of absorption peaks corresponding to functional groups of organic compounds was based on relevant scientific literature, as shown in Table 1.

An index, calculated as the ratio between peaks at 2853 and 2923 cm^{-1} (CH_2–Index), was proposed to characterize compounds related to symmetric and asymmetric CH_2 vibrations. Observation of the CH_2 stretching intensities reveals that asymmetric vibrations are greater than symmetric vibrations. As chain length/molecular weight increases, there is a decrease in methyl contribution and an increase in methylene contribution. The molecular symmetry of the compound significantly impacts the spectrum, along with factors such as relative electronegativity, bond order, and the relative mass of participating atoms. Therefore, the goal was to investigate whether the proportion of compounds associated with these peaks exhibits linear and spatial correlations with

Table 1
FTIR vibrational assignments for soil organic matter absorbances sample.

Frequency range	Absorption (cm^{-1})	Peak	Associated group	References
Band A				
3000–2840	2941	I	CH_3 asymmetric stretch	[a], [b], [c], [d]
	2923	II	CH_2 asymmetric stretch	[a], [b], [c], [d]
	2900	III	Aldehyde C-H stretch	[a], [b], [c], [d]
	2894	IV	CH stretch	[a], [b], [c], [d]
	2872	V	CH_3 symmetric stretch	[a], [b], [c], [d]
	2853	VI	CH_2 symmetric stretch	[a], [b], [c], [d]

[a] Senesi et al. (2007).
[b] Piccolo et al. (1992).
[c] Tatzber et al. (2007).
[d] Coates (2001).

the evaluated soil attributes. All data processing was performed using the R version 4.2.0 program (Liland, 2016; Liland and Mevik, 2015) and OMNIC™ software.

2.5. Soil attributes

Field measurements of CO_2 flux (CO_2–F) from the soil were conducted during May and June (05/05/2018; 05/31/2018; 06/05/2018; 06/14/2018, and 20/06/2018) using portable LiCor systems (LI–8100), as explained by Tavanti et al. (2020b). The systems were attached to polyvinyl chloride (PVC) collars measuring 8.5 cm in height and 10 cm in diameter, which had been previously installed at the sampling points of the georeferenced sampling grids. Soil CO_2 emissions were measured over a 5-min interval. The CO_2 emission for this period was estimated by calculating the area under the curve (AUC) formed by the function that describes the emission over time. The average values of emissions over the evaluation days are included in the Supplementary Files (Fig. A.1).

For the collected soil samples, pH measurements were performed using a $CaCl_2$ solution according to the method described by Van Raij et al. (2001). Clay, silt, and sand content was determined using the pipette method (Embrapa, 2017). Organic carbon content was calculated according to the method of Cambardella et al. (1994). After the soil sample is passed through a 0.053 mm sieve, particulate organic carbon (POC) is separated from organic carbon (MAOC) associated with the mineral fraction. Only POC content is measured, while MAOC is determined by calculating the difference between total organic carbon (TOC) and POC. To determine TOC and POC content, 10 mL of 1 mol $L^{-}1$ HCl was added to 10 g of soil to remove carbonate (inorganic carbon in limestone). After this process, the floors are dried in an oven at 60 °C for 15 h. Dried soils were macerated and analyzed according to the method proposed by Yeomans and Bremner (1988).

From the 10 g sample used for TOC determination, 5 g was used for particle size separation of MAOC and POC. These fractions were determined using the same method as for TOC. Stocks of TOC (TOC-S), POC (POC-S), and MAOC (MAOC-S) were calculated according to the method of Soares et al. calculated Soares et al. (2020), where the content of each fraction is multiplied by soil bulk density and soil depth, as shown in Eq. (1):

$$\text{C stocks}\left(\text{Mg ha}^{-1}\right) = \text{C}\ (\%) \times \text{Soil depth}\ (\text{m}) \times \text{Bulk density}\left(\text{Mg m}^{-3}\right) \times 100 \quad (1)$$

To facilitate a comparison of carbon stocks among equal soil masses, corrections were calculated using the equivalent soil mass method (Ellert and Bettany, 1995), with the soil bulk density of native forest areas serving as a reference. The corrected stocks were estimated through an adjustment that incorporated the corrected depth (Depth. Corr.), as determined by Eq. (2):

$$\text{Depth.Corr.}(\text{m}) = \frac{\text{BD}_\text{r}}{\text{BD}_\text{c}} \times \text{Depth ref.} \quad (2)$$

where: BD_r represents the bulk density of the reference soil (native forest) near the sampling area (Mg m^{-3}), BD_c represents the bulk density requiring correction (Mg m^{-3}), and Depth. ref. represents the reference depth for equal masses. These soil parameters were obtained from a previous study conducted by Tavanti et al. (2020a) and were utilized to investigate the multivariate relationship between the soil attributes and FTIR spectra.

2.6. Statistical analysis

Descriptive analyses and the Shapiro-Wilk normality test ($p < 0.05$) were performed on the set of analyzed variables. Outliers were identified and removed from the dataset based on values that exceeded three times the interquartile range. A comparison of means between the grassland management systems was conducted using the bootstrap technique, which involved 1000 random resamplings with replacement, following the method proposed by Tavanti et al. (2020b). From the resulting 1000 values, the upper and lower limits of the confidence interval for the means were determined, encompassing a 95% probability. These confidence intervals were used for subsequent comparisons of means. If the confidence intervals overlapped or the error bars touched, the means were considered not significantly different, while the absence of overlapping values indicated significant differences ($p < 0.05$).

The study did not employ a specific statistical design; therefore, a multivariate statistical method was chosen to examine the impact of management systems on the analyzed variables. In order to mitigate the influence of unit factors, such as scale differences on the study results, the dataset was standardized. This standardization ensured that all variables contributed equally to the calculation of the similarity coefficient between sampling units (Wilks, 2006). The following equation was used to standardize the variables for the analysis:

$$Z_{ij} = \frac{X_{ij} - \overline{X}_j}{S_j} \quad (3)$$

where X_{ij} is the value of the ith access of variable j; $\overline{X}_j$ is the original mean of the j^{th} variable; S_j is the standard deviation, and Z_{ij} is the value of the standardized variable.

To ensure the appropriate application of Principal Components Analysis (PCA), the data were subjected to the Kaiser-Meyer-Olkin's test (with a threshold of ≥0.50) and Bartlett's sphericity test ($p < 0.05$) to verify the fulfillment of basic assumptions. The commonality of the variables was also assessed, and any variables with values below 0.50 were removed from the analysis. Principal Components (PCs) with eigenvalues >1.0 were selected for further analysis. In order to provide a clear visualization of the first three extracted PCs, a triplot graph was generated, depicting the load of each attribute as arrows and the scores of each treatment as points. Additionally, a Pearson's correlation heatmap was computed to examine the relationships among the variables under the proposed management systems.

Multivariate data analysis was used to synthesize the number of variables without reducing information. Therefore, the scores of the first three PCs were used to map the soil attributes in the two areas. The spatial dependence of Band A organic compounds, soil attributes, and new synthetic variables (scores) was assessed using semivariograms. The Exponential, Gaussian, and Spherical semivariogram models were also tested. The model selection criteria were highest coefficient of determination (R^2), lowest root mean square error (RMSE), and linear coefficients close to zero and slope close to one in the cross-validation process (Qin et al., 2019; Yao et al., 2019). The spatial variability dependence was classified based on the nugget-to-plateau ratio (Cambardella et al., 1994).

2.7. Machine learning approach

A chemometric model, as described by Mohanty et al. (2016), was employed to identify relationships between soil respiration × FTIR spectra and soil attributes, with the aim of determining the most significant spectral bands for this purpose. The procedure involved fitting a Random Forest (RF) model, where CO_2–F served as the dependent variable and spectral data and soil attributes were utilized as predictors. RF was chosen due to its advantageous characteristics when compared to other machine learning techniques. It is a non-parametric method, capable of handling datasets with a higher number of predictors than observations while avoiding overfitting (Díaz-Uriarte and De Andres, 2006; Wiesmeier et al., 2011). Additionally, RF is well-suited for addressing small-n large-p problems and exhibits robustness against noise and outliers (Guio Blanco et al., 2018).

In this study, we leveraged the spatialized information (maps) of the analyzed variables to refine the model adjustment. A total of 5570 samples (pixels) were obtained in the managed grassland area, while 3703 samples were collected in the unmanaged grassland area. To calibrate and validate the model, the data from the interpolated maps were divided into training and test sets. Approximately 70% of the samples were randomly selected for model construction (training set), while the remaining 30% were used for validation (test set). A 10 k-fold cross-validation strategy was employed to evaluate the RF model performance on both datasets. To perform the validation, the dataset was divided into k folds, and at each run, k-1 folds were used to train, and the remaining fold was used to validate the model. This process repeats k times; thus, all folds were used for both training and validating the model. We applied 1000 trees, and the maximum number of features at each split had been determined through grid search optimized to find the best performance. RF was calculated with the "caret" package in R environment.

The performance of the model was assessed by comparing the predicted values with the observed data in the test set. Several parameters were calculated to evaluate the model's performance, including the R^2, mean squared error (MSE), RMSE, and mean absolute error (MAE):

$$R^2 = 1 - \frac{SS_{error}}{SS_{total}} \quad (4)$$

$$MSE = \frac{1}{n}\sum_{i=1}^{n}(Y_i - \hat{Y}_i)^2 \quad (5)$$

$$RMSE = \sqrt{MSE} \quad (6)$$

$$MAE = \frac{1}{n}\sum_{i=1}^{n}|Y_i - \hat{Y}_i| \quad (7)$$

where Y_i and $\hat{Y}_i$ represent the observed and predicted CO_2–F at point *i*, respectively; *n* is the number of observations in the model; and SS is the sum of the square values.

All statistical analyzes were performed with the R software version 4.2.0 and the packages "nortest," "agricolae", "geoR", "factoextra", "gstat" and "caret". The kriging maps were edited using QGIS 3.28.3 software.

3. Results

3.1. Visual and descriptive analysis of FTIR spectra and soil attributes

The FTIR spectra of the soil samples exhibited absorption signals in the frequency range associated with SOM, specifically within the range of 2955 to 2830 cm^{-1}, which corresponds to aliphatic C—H stretching (Fig. 3B; Table 2). Notably, two distinct peaks were observed at 2923 cm^{-1} (Peak II) and 2853 cm^{-1} (Peak VI), which were attributed to

Table 2
Descriptive analysis of soil attributes obtained from the integral IR absorbance intensity of the FTIR spectra (arbitrary units) and normality test under different livestock farming systems.

Attribute	Mean	Median	Min	Max	SD[1]	CV[2]	Coefficient		S-W[3]	Pr ≥ Fc[4]	Bootstrap comparison's test[5]	
							Kurtosis	Skewness			Unmanaged grass.	Managed grass.
Soil physical												
Clay (g kg^{-1})	128.36	126.54	98.80	164.81	10.424	7.9	0.19	1.47	0.00 *	0.06 ns	131.01 A	126.13 A
Silt (g kg^{-1})	61.43	68.17	17.43	95.13	20.597	31.7	−0.56	−0.74	0.00 *	< 0.001*	47.20 B	73.47 A
Sand (g kg^{-1})	810.62	808.90	764.99	872.75	22.521	2.7	0.26	−0.37	0.26 ns	< 0.001*	822.16 A	800.86 B
Soil chemical												
pH $CaCl_2$	5.16	5.10	4.40	6.30	0.410	7.6	0.41	−0.44	0.00 *	< 0.001*	4.9 B	5.4 A
CO_2-F (μmol m^{-2} s^{-1})	1.170	0.980	0.940	1.540	0.221	18.9	0.22	−1.90	0.00 *	< 0.001*	1.40 A	0.97 B
TOC-S (Mg ha^{-1})	16.67	16.71	14.79	18.86	0.788	4.7	−0.04	0.03	0.72 ns	< 0.001*	16.24 B	17.03 A
POC-S (Mg ha^{-1})	6.50	6.43	5.26	8.06	0.629	9.7	0.31	−0.68	0.02 ns	0.68 ns	6.52 A	6.48 A
MAOC-S (Mg ha^{-1})	10.17	10.26	7.72	11.98	0.774	7.6	−0.53	0.37	0.05 ns	< 0.001*	9.72 B	10.55 A
Band A												
Peak I	0.007	0.007	0.000	0.011	0.003	46.9	0.32	−1.01	0.87 *	0.003*	0.005 B	0.007 A
Peak II	0.123	0.115	0.052	0.253	0.041	33.2	0.20	0.67	0.96 *	< 0.001*	0.142 A	0.105 B
Peak III	0.007	0.007	0.000	0.014	0.003	49.7	0.16	−0.60	0.92 *	< 0.001*	0.005 B	0.007 A
Peak IV	0.008	0.008	0.000	0.016	0.004	51.6	−0.20	−0.46	0.94 *	< 0.001*	0.005 B	0.009 A
Peak V	0.032	0.035	0.000	0.059	0.015	45.5	0.52	−0.97	0.89 *	< 0.001*	0.024 B	0.039 A
Peak VI	0.039	0.036	0.011	0.087	0.017	42.8	−0.48	0.51	0.96 *	< 0.001*	0.048 A	0.030 B
Index												
CH_2 index	0.322	0.315	0.195	0.811	0.074	23.0	14.64	2.51	0.83 *	< 0.001*	0.359 A	0.285 B

ns Not significant.
[1] SD: standard deviation.
[2] CV: Coefficient of variation (%).
[3] S-W: W value obtained from the Shapiro-Wilk test (W ≤ 0.05).
[4] Pr ≥ Fr: *p*-value obtained from ANOVA.
[5] Uppercase letters classify pasture management systems by the confidence intervals obtained in the bootstrap test at 0.05 probability.
* Significant at 0.05 probability.

symmetric and asymmetric CH_2 bonds, respectively (Fig. 4). Upon applying second derivative and deconvolution techniques to the spectra, four additional peaks became evident within Band A, occurring at frequencies of 2941 (Peak I), 2900 (Peak III), 2894 (Peak IV), and 2872 cm^{-1} (Peak V). These peaks were associated with the vibrations of asymmetric CH_3, CH aldehyde, CH stretch, and CH_3 symmetric bonds, respectively.

Based on the descriptive analysis (Table 2), the compounds related to functional groups exhibited a frequency distribution classified as "non-normal" according to the Shapiro-Wilk test, indicating a wide range of values spanning from the minimum to maximum. Notably, the compounds associated with the vibrations of Peaks III and IV displayed the highest variability within Band A, with coefficients of variation of 51.6% and 49.7%, respectively. Despite the significant variability, the median values aligned with the overall mean, indicating a tendency towards normality. When comparing the different management systems, the unmanaged grassland exhibited the highest values for Peaks II and VI. This finding was attributed to a reduction of 37.5% and 26% in the compounds associated with Peak VI and II, respectively, in comparison to the managed grassland system. In contrast, higher-energy aliphatic compounds (Peaks I and V) demonstrated greater relative abundance in the managed grassland system.

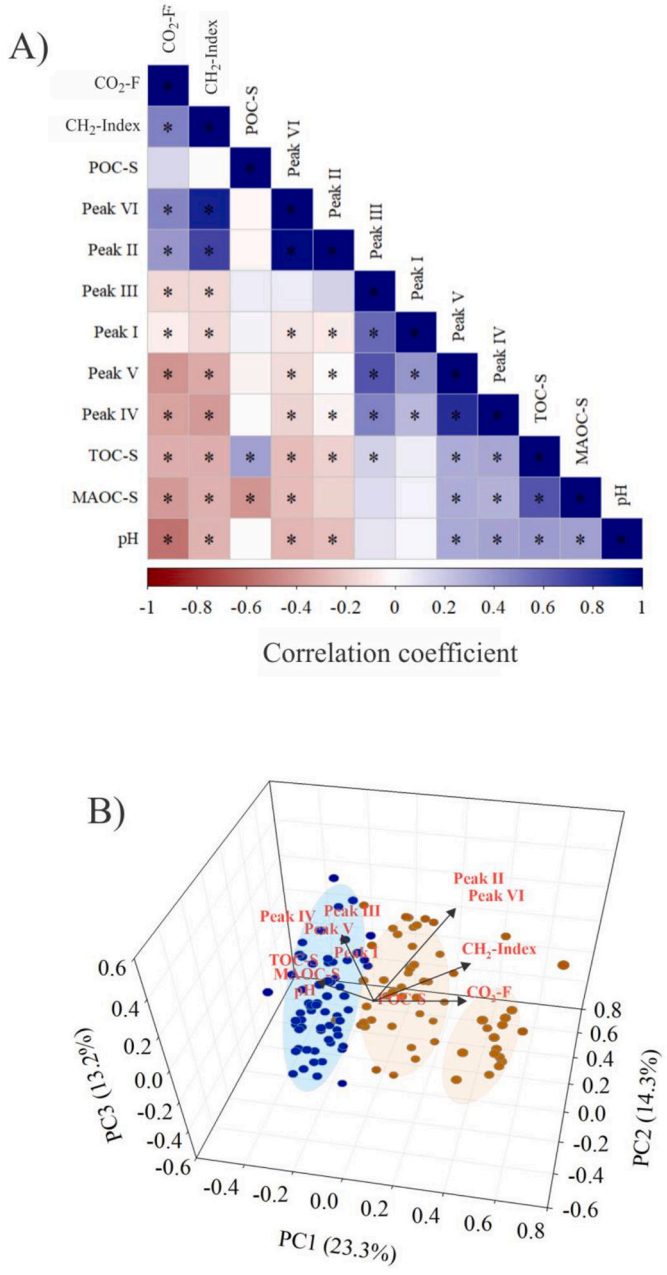

Fig. 4. Heatmap of Pearson correlations ($p < 0.05$) between analyzed soil attributes (A). * Indicates significant correlation. Principal component analysis (PCA) triplot showing the loading of each soil attribute (arrows) and the scores of each livestock farming system (points) (B). Nearby points correspond to observations that have similar scores on the PCA components. The length of the arrows indicates the variance of the attributes in the component, while the points between them indicate their correlations. The blue circle indicates the grouping of managed grassland and the brown circle unmanaged grassland grouping.

Regarding the remaining attributes, the descriptive analysis revealed values of TOC-S were classified as satisfactory, surpassing 12 Mg ha^{-1} in both evaluated systems. The managed grassland area showed a higher accumulation of carbon, up to 5% (~ 0.8 Mg ha^{-1}) (Table 2). The adopted management system, characterized by extensive livestock with a moderate stocking rate, proved beneficial for carbon accumulation in the surface soil horizons. This increase was primarily attributed to the more decomposed physical fraction (MAOC-S), also known as the heavy fraction, which accounted for the majority of TOC-S, representing 59.9% in the unmanaged grassland area and 62% in the managed grassland area. Conversely, POC-S stocks did not differ significantly between the evaluated pasture management systems. Regarding soil respiration (CO_2-F), emissions were lower in the managed grassland area, with an average of 0.97 μmol m^{-2} s^{-1}. The observed reduction in CO_2-F in the unmanaged grassland area reached up to 31%. Both study areas exhibited a loamy sand texture class with minimal variation in clay content (131 and 126 g kg^{-1}). Thus, the clay content, which could potentially influence soil carbon content, was not identified as a major factor in this study, likely due to its role in physically protecting soil organic matter (Bruun et al., 2015; Miranda et al., 2016). The heatmap of Pearson's correlation coefficients further revealed a positive correlation between CO_2-F and Peak VI ($R = 0.51$*) as well as Peak II ($R = 0.44$*) (Fig. 4A). There was also a strong negative correlation between CO_2-F and pH $CaCl_2$ (−0.55*).

Regarding the correlations obtained with carbon stocks, significant correlations were observed between MAOC-C and TOC-S (0.65*), CO_2-F (−0.39*), pH $CaCl_2$ (0.37*), Peak VI (−0.25*), Peak V (0.31*), and Peak IV (0.29*) (Fig. 4A). TOC-S exhibited a similar trend to MAOC-S concerning the peaks, suggesting that it was the fraction responsible for the variation of the compounds observed in the FTIR spectra.

A wide range of values was observed for the majority of the variables assessed (Table 2). Coefficients of variation were also high, exceeding 30% for most variables, except for clay, sand, pH $CaCl_2$, TOC-S, MAOC-S, POC-S, and CO_2-F. The Shapiro-Wilk test also confirmed a "non-normal" distribution for most of the attributes examined. However, it was observed that the data for clay, silt, pH $CaCl_2$, and CO_2-F exhibited a distribution that tended towards normality, as evidenced by the similarity between the mean and median values, as well as the close-to-zero values of asymmetry and kurtosis.

3.2. Multivariate approach

PCA was performed, extracting four components (PCs) with eigenvalues above 1.0, ranging from 2.247 to 1.135, collectively explaining 62.6% of the total dataset variability (Table 3). The first PC accounted for 23.3% of the explained variance and exhibited positive correlations with CO_2–F, Peak V, and CH_2–Index while displaying negative correlations with Peaks I, III, IV, and VI. This component represented the organic compounds associated with soil CO_2 emissions in the evaluated management systems. The second PC explained 14.3% of the variance and showed positive correlations with compounds associated with Peaks I and III, and negative correlation with MAOC–S. The third PC explained 13.2% of the variance and represented TOC accumulation driven by MAOC–S and prominent organic compounds in the soil. In this

Table 3
Summary of the principal components obtained from the PCA of the attributes and FTIR spectra of an Oxisol under different livestock farming systems.

Summary	Principal component			
	PC1	PC2	PC3	PC4
Eigenvalue	2.247	1.382	1.279	1.135
Explained variance (%)	23.3%	14.3%	13.2%	11.8%
Accumulated variance (%)	23.3%	37.6%	50.8%	62.6%
Variables	Correlation[1]			
Soil attributes				
pH $CaCl_2$	−0.23	−0.26	0.22	0.14
CO_2-F	**0.33***	0.29	−0.14	0.00
TOC-S	−0.25	−0.22	**0.31***	**0.49***
POC-S	−0.02	0.19	−0.16	**0.83***
MAOC-S	−0.23	**−0.37***	**0.43***	−0.18
Band A				
Peak I	**−0.30***	**0.39***	−0.07	−0.11
Peak II	0.27	0.24	**0.52***	0.02
Peak III	**−0.30***	**0.45***	0.12	−0.04
Peak IV	**−0.35***	0.24	0.16	−0.06
Peak V	**0.31***	0.26	**0.44***	0.02
Peak VI	**−0.37***	0.29	0.13	−0.07
Index				
CH_2 index	**0.34***	0.05	**0.32***	0.07

[1] * Indicates significant correlation in the principal component.

component, TOC–S, MAOC–S, Peaks II and V, and CH_2–index was positively correlated. Finally, the fourth PC explained 11.8% of the variance and displayed positive correlations between TOC–S, and POC–S.

To better understand the correlation between FTIR spectra organic compounds, soil attributes, and CO_2–F within the components, a PCA triplot was constructed (Fig. 4B). The position of treatment scores and arrows characterizing the variance of CO_2–F, Peaks II and VI, and CH_2–Index indicated a higher occurrence of elevated CO_2–F values in the unmanaged system. Similarly, lower pH $CaCl_2$ values and decreased occurrence of Peaks III, V, and IV were observed in this system. The managed grassland exhibited a higher occurrence of elevated MAOC-S and pH $CaCl_2$ values, and a greater relative abundance of compounds associated with Peaks I, III, IV, and V. In the triplot chart, it was possible to distinguish the scores of the management systems. Only a few points are in the scoring transition zone, indicating similar regions. From the spatial analysis, it is possible to verify if these points (scores) are regionalized to delimit specific management zones.

3.3. Geostatistical analysis

The results of the geostatistical analysis, including adjusted semivariograms of principal component scores, FTIR spectra organic compounds, and soil attributes, are presented in the Supplementary Files (Table A.1). In summary, the extracted components and soil attributes exhibited spatial dependence, except for Peaks I and IV in the unmanaged grassland area, silt, sand, Peaks I, II, and IV in the managed grassland area. The goodness of fit of the semivariogram models was confirmed by R^2 and RMSE. Linear coefficients close to zero and slopes close to one were observed during cross-validation for all evaluated attributes. Based on the adjusted semivariograms, ordinary kriging was used to interpolate all variables, which were then represented in maps with values classified into equidistant classes.

The maps of soil attributes clearly revealed differences between the management systems (Fig. 5). In the unmanaged pasture system, locations with CO_2–F reaching 1.64 μmol m^{-2} s^{-1} and MAOC–S stocks below 8.0 Mg ha^{-1} were observed. In contrast, locations with TOC–S values close to 18.0 Mg ha^{-1} showed CO_2–F of 0.97 μmol m^{-2} s^{-1}, equivalent to the condition of the managed grassland system. The CO_2–F, TOC–S, and MAOC–S maps confirmed the spatial correspondence in the unmanaged pasture area.

The attributes related to C exhibited different behaviors in the managed grassland area (Fig. 5). In locations with good fertility conditions (represented by the values >5.3 in pH $CaCl_2$ map), emissions of 0.99 μmol m^{-2} s^{-1} were recorded as the highest values. The CO_2–F values in this system ranged between 0.94 and 0.98 μmol m^{-2} s^{-1}. Locations with TOC–S between 15.5 and 18.5 Mg ha^{-1} corresponded to POC–S values between 5.5 and 8.0 Mg ha^{-1} and MAOC–S values between 9.0 and 12.0 Mg ha^{-1}, representing sites with the highest stocks and CO_2 emissions.

The PC1 maps clearly exhibited distinct score distributions between the managed and unmanaged pasture systems (Fig. 7A). In the unmanaged pasture system, regions with high concentrations of organic compounds associated with Peak V displayed the highest CO_2 emissions (indicated by positive scores on the PC1 maps). The CH_2–Index also followed these findings, showing a correlation with the component (0.34*). Regions with scores >0.13 represented critical values of CO_2–F, ranging from 1.36 to 1.49 μmol m^{-2} s^{-1}, and Peak V from 0.00 to 0.029 a.u (Figs. 5 and 7). In the renovated grassland, PC1 scores ranged from −0.16 to −0.01, indicating variations in CO_2–F between 0.94 and 0.98 μmol m^{-2} s^{-1} and Peak V from 0.031 to 0.059 a.u. The CH_2–Index ranged from 0.24 to 0.32 in this system, regardless of the emission patterns. In the unmanaged grassland, 85.7% of the area exhibited scores above 0.13, indicating the highest emission rates (> 0.98 μmol m^{-2} s^{-1}) and low concentrations of organic compounds associated with Peak V (< 0.029 a.u.). Peaks III and VI, on the other hand, indicated regions with contrasting behavior compared to other attributes correlated in PC1. Values ranging from 0.0068 to 0.0084 a.u. and 0.026 to 0.029 a.u. were observed in areas with higher CO_2 emissions (> 1.37 μmol m^{-2} s^{-1}), suggesting specific accumulation patterns under these conditions.

The PC2 maps displayed the spatial distribution of scores associated with Peak III compounds and MAOC–S, revealing a clear separation between regions with high and low concentrations in both study areas (Fig. 6B). Locations represented by scores below zero (indicated by yellow-blue colors) exhibited MAOC–S ranging from 10.24 to 11.98 Mg ha^{-1} in the managed grassland, and 10.03 to 10.52 Mg ha^{-1} in the unmanaged grassland. These values represented the highest concentrations in both areas, with a greater extent in the managed pasture system (84.3% coverage). Conversely, the concentrations of compounds related to Peak III exhibited inverse distribution patterns, ranging from 0.0068 to 0.079 a.u. in the managed pasture area and 0.0042 to 0.0053 a.u. in the unmanaged pasture area. Notably, there were similarities between the maps of this component and the MAOC–S and Peak III maps. However, a spatial comparison with Peak I was not possible due to the lack of spatial dependence.

Regarding the PC3 map, the spatial distribution scores indicated correlations between the concentrations of Peaks II and V-related compounds and MAOC–S and TOC-S stocks (Fig. 6C). In the managed grassland system, Peak II values fluctuated between 0.09 and 0.11 a.u. in locations with scores above 0.01, while Peak V from 0.031 to 0.040 a.u. In this range of scores, we have the highest accumulations of the evolved fraction of C (MAOC–S > 10.39 Mg ha^{-1}) and highest concentrations of compounds related to Peak V. On the other hand, compounds associated with peak II exhibited an inverse pattern, with low concentrations in locations of higher C stocks. In the unmanaged pasture area, a region with scores below −0.06 was clearly defined in the center of the map, indicating similarity with the MAOC–S map (Fig. XX). In this sense, the lowest values of stocks were observed, < 9.89 Mg ha^{-1}. The same behavior can be observed in the Peak II map of this system, however with an accumulation behavior, with values ranging from 0.117 to 0.133 a.u. A visual correspondence between the PC2 and PC3 maps was evident, due to the region with low MAOC–S stocks.

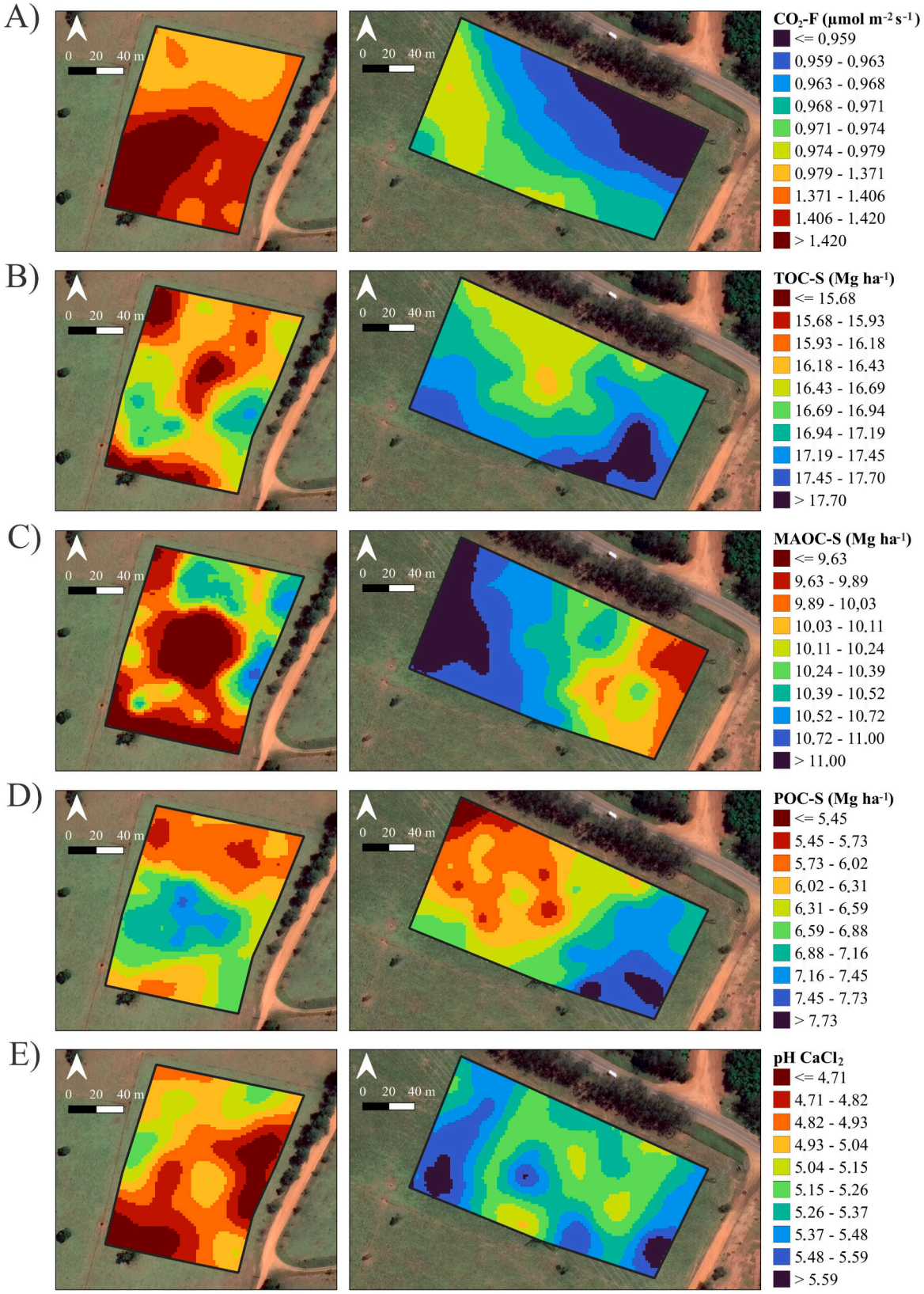

Fig. 5. Spatial distribution of the soil chemical attributes (CO_2-F – A; TOC-S – B; POC-S – C; MAOC-S – D and pH $CaCl_2$ – E). The left maps correspond to the unmanaged grassland and the right maps to the unmanaged grassland.

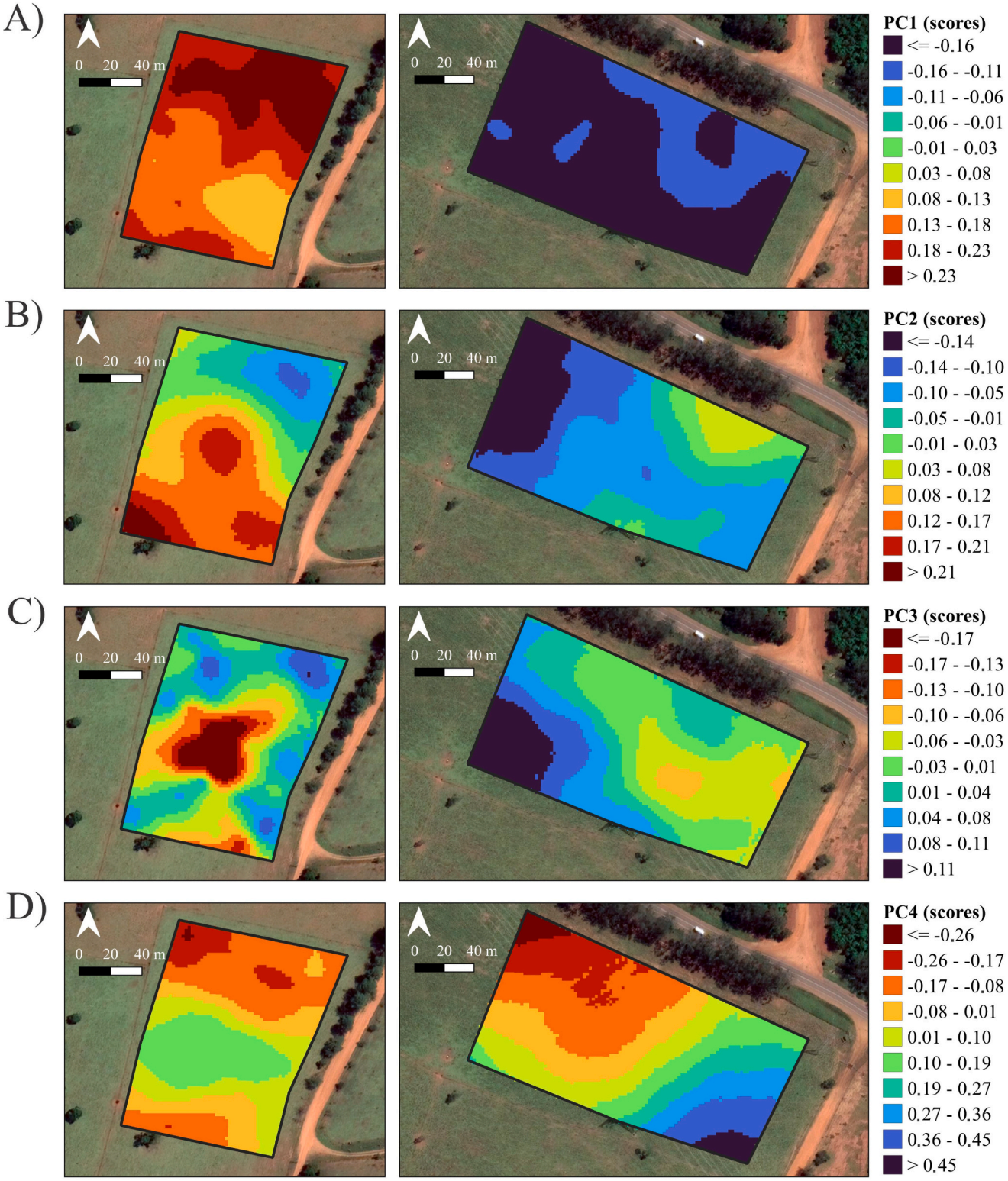

Fig. 6. Spatial distribution of the principal components obtained (PC1 – A; PC2 – B; PC3 – C and PC4 – D), represented by the organic compounds of Band A and chemical attributes of the soil. The left maps correspond to the unmanaged grassland and the right maps to the unmanaged grassland.

3.4. Machine learning approach

Based on the evaluation metrics of the RF model, an excellent fit was achieved for CO_2-F predictions, as indicated by an R^2 value of 0.98, demonstrating low variability compared to the observed data (Fig. 8A). The model exhibited a low average error, with an RMSE of 8.7×10^{-4} and MAE of 3.8×10^{-4}. The scatter plot depicting observed and predicted CO_2-F values showed a close alignment of training and test scores along a 1:1 line. The separation between the pasture management systems was evident, with the unmanaged pasture area displaying higher values, greater amplitude, and increased dispersion. In terms of variable importance, it was apparent that spectral information played the most

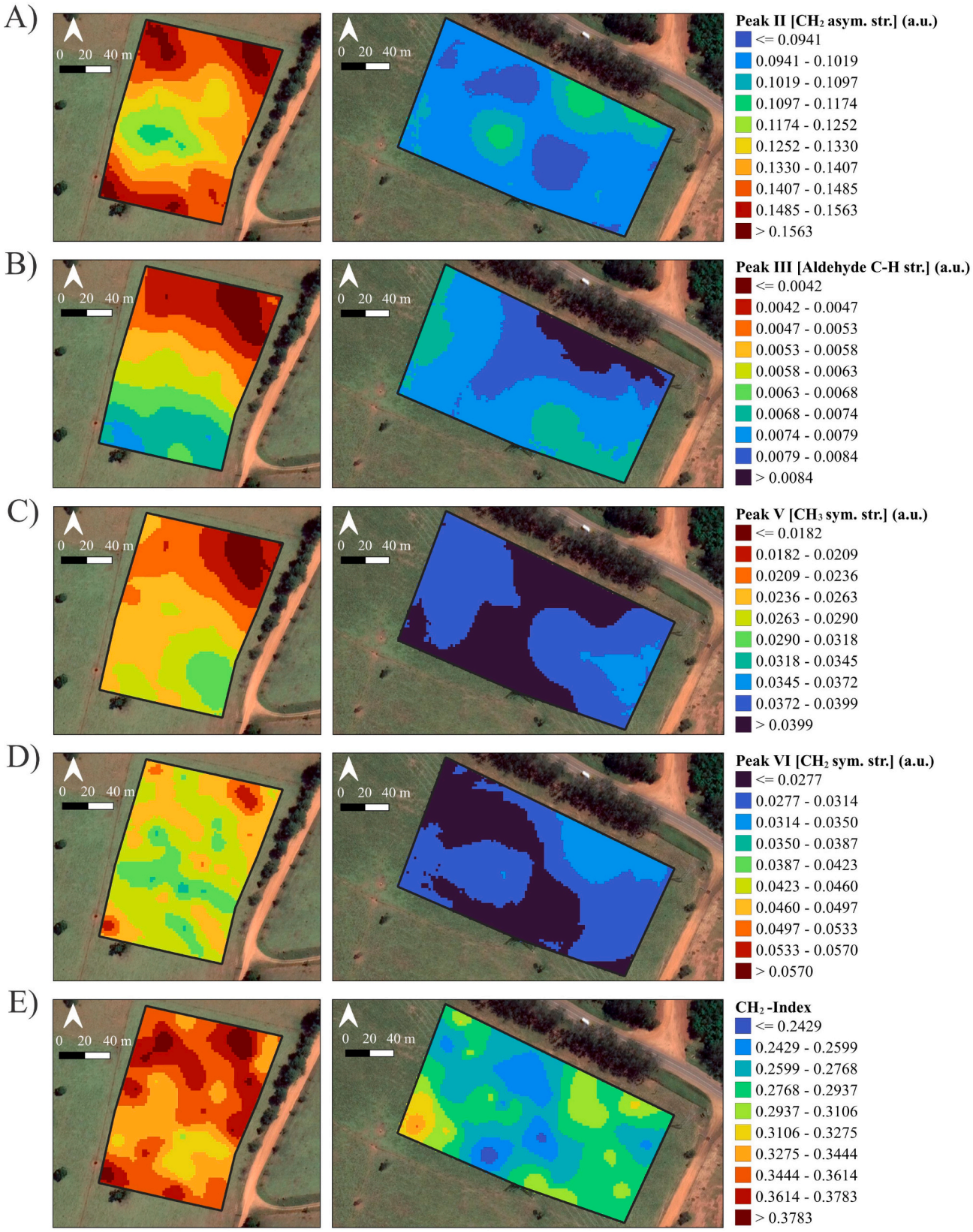

Fig. 7. Spatial distribution of the peaks of organic compounds extracted by FTIR spectra. The left maps correspond to the unmanaged grassland and the right maps to the unmanaged grassland.

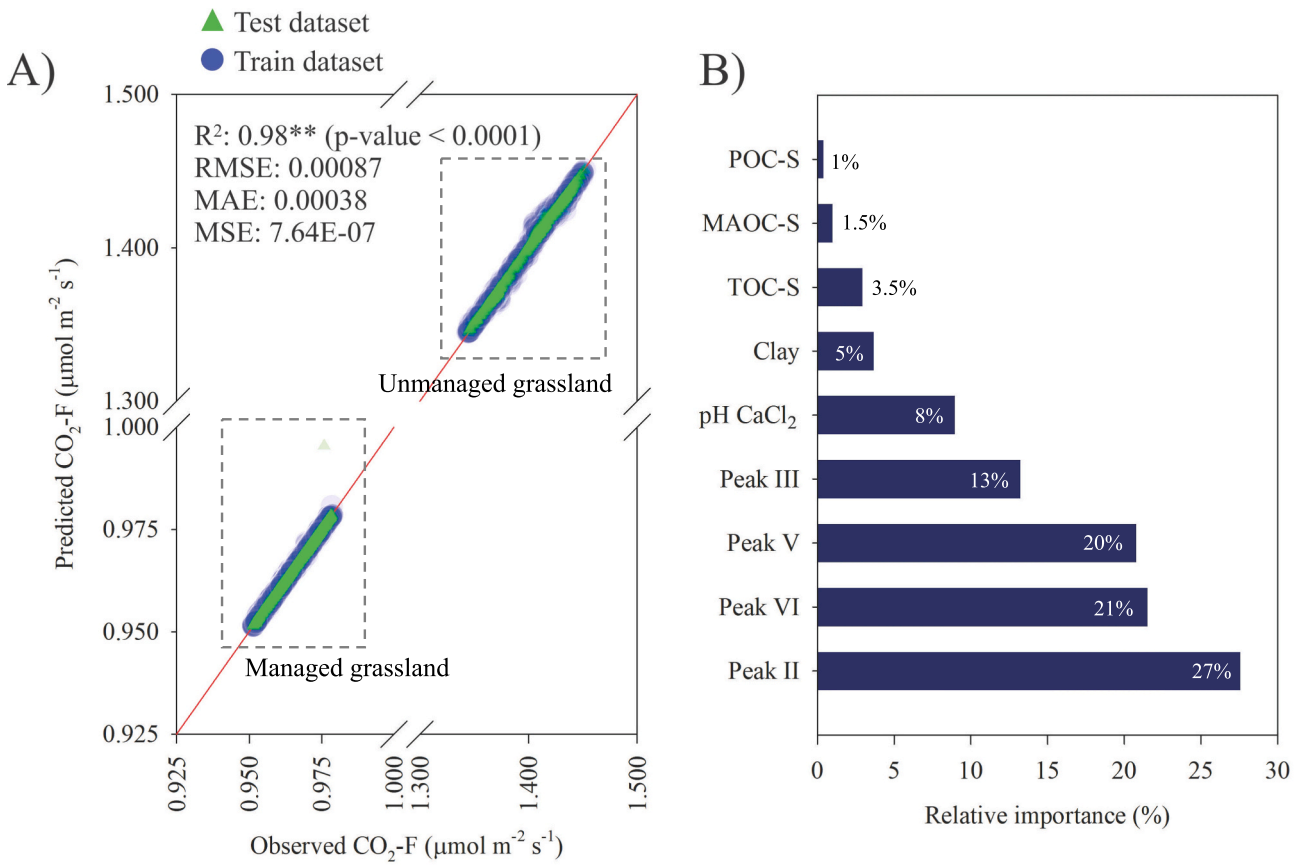

Fig. 8. Scatter plots of the observed and predicted CO_2-F (µmol m^{-2} s^{-1}) in two different livestock farming systems. (B) The relative importance of soil attributes variables and organic compounds obtained from FTIR spectra. Peak II (2923 cm^{-1}), Peak III (2900 cm^{-1}), Peak V (2872 cm^{-1}) and Peak VI (2853 cm^{-1}).

significant role in predicting soil CO^2 emissions (Fig. 8B). The most influential contributors, in descending order, were Peaks II (27%), VI (21%), V (20%), and III (13%). Clay and pH $CaCl_2$ contents also had a moderate impact, with weights 5% and 8% higher, respectively, compared to carbon stocks, which accounted for <4% of the overall importance.

4. Discussion

Through visual evaluation of the FTIR spectra, it was possible to observe alterations in the peaks of Bands A, which were correlated to the management systems and sampling locations. The spectral signatures that effectively characterized the systems were obtained at frequencies of 2923, 2900, and 2853 cm^{-1}, due to the intensity of peaks associated with asymmetrical CH_2, symmetric CH_2 and aldehyde C—H groups, respectively (Fig. 4B).

The clay content has the potential to influence soil C levels through organo-mineral interactions (Bruun et al., 2015; Miranda et al., 2016). In highly weathered soils, such as the one investigated in this study, the sorption of SOM can occur at the edges of kaolinite particles, where more reactive sites, such as aluminol groups, are present (Sposito, 1989). However, we believe that this effect may not have been the predominant factor influencing the concentrations of compounds in Band A or the accumulation of C stocks in the study areas. This is attributed to the low clay content (~126 g kg^{-1}) and cation exchange capacity (40.5 $mmol_c$ dm^{-3}) of the soil under investigation, as well as their low relative importance in the machine learning model and the variability observed between the different pasture management systems (Table 2). Therefore, we assume that the minor changes observed in this group of compounds are inherent to the operations conducted during pasture renovation, particularly the application of limestone and its incorporation into the soil profile.

The vibrational region of 2800–3000 cm^{-1} may indicate the presence of organic compounds such as branched alkanes (Allen et al., 1994), aldehydes, compounds containing methylene groups (Reitner et al., 2011), hydrocarbons and other aliphatic compounds. In general, many of these compounds have low molecular weights. The decomposition of organic matter is a complex and dynamic process that involves the action of a variety of decomposing microorganisms and environmental factors. There is no hard and fast rule that determines which compounds are broken down first. However, in general terms, low molecular weight organic compounds tend to be more easily decomposed by microorganisms present in the soil. This is because these compounds are more accessible and provide a more readily available source of energy for decomposers (Cotrufo et al., 2015).

The CO_2–F emissions exhibited a strong correlation with the presence of symmetrical and asymmetrical CH_2 compounds (Peak II and VI). The PC1 map revealed that the unmanaged pasture area displayed the highest concentrations of symmetrical CH_2 compounds, accompanied by increased CO_2–F emissions, delineating areas of particular interest (pixels in dark red) (Fig. 6A). In contrast, the managed pasture system exhibited lower concentrations of these compounds and, consequently, lower CO_2–F rates. It is hypothesized that the stretching of CH_2 bonds is closely linked to CO_2–F emissions due to two potential mechanisms: *(i)* the introduction of less labile and aliphatic-poor molecules, such as those found in sorghum residues from silage production, which can induce changes in microbial communities and alter the dynamics of SOM decomposition, and *(ii)* conformational changes in functional groups within SOM under varying pH conditions. Previous studies have demonstrated the significance of pH and ion concentrations in the aggregation of SOM (Hurraß and Schaumann, 2006; Pimentel et al., 2019). A high ionic strength in the soil solution can bring charged functional

groups of SOM closer together, potentially leading to molecular conformational changes that offer partial protection to certain groups of molecules on the surface.

The forms of net loss of aliphatic compounds in agricultural systems were described by Pimentel et al. (2019), who studied the dynamics of the decomposition of sugarcane straw. The authors found that labile C fractions (aliphatic compounds) possibly were preferentially consumed by the soil microbiota during the initial SOM decomposition process. The intermediate fractions of decomposable C, as stable compounds, tended to become prominent. Thus, the relative concentration of lignin tended to increase, and aliphatic compounds decreased in the remaining SOM (José et al., 2017).

In agricultural systems that cultivate forage species, the material supplied comes from cultural residues from pastures, except in some cases when there are rotations/ successions of other cultures to renovate the pastures. Organic waste from the rest of the pasture has a high C:N ratio (> 20:1) (Guo et al., 2012; Torres et al., 2005), high cellulose concentrations (between 245 and 340 g kg^{-1}), and lignin (between 60 and 80 g kg^{-1}) (Herrero et al., 2001). Complex organic polymers, such as lignin, are highly resistant to degradation (Kögel-Knabner, 2002). Only specialized microbiota (predominantly fungi) can synthesize extracellular enzymes (such as peroxidases and laccases) that break down highly stable structures into biologically accessible forms (Swift et al., 1979; Arantes and Milagres, 2009). Furthermore, lignin limits the access of microbial enzymes to the more labile polysaccharides present in the cell wall (Pauly and Keegstra, 2008), thus playing an important role in regulating the decomposition of straw. Lignin accounts for approximately 30% of the C sequestered in plant materials annually (Boerjan et al., 2003). Together with cellulose, lignin can control the speed at which the decomposition process of the straw takes place, which drives the intensity of the C fluxes in the soil-atmosphere system (Schwarz, 2001).

Checking our results with other studies using the same land use and only changing management, soil carbon accumulation after management (0.78 t ha^{-1}) was 122% higher than the UNCCD recommended average (0.35 t ha^{-1}). Depends on climate region (0.02–0.8 t ha^{-1}), remaining within limits (Sanz et al., 2017). Compared to other land uses (agriculturally restored ecosystems), soil carbon accumulation rates are 0.15 t ha^{-1} in dry and hot regions (Armstrong et al., 2003), and 0.1–1 t ha^{-1} in humid regions with cold climates region (West and Post, 2002), our results are larger than expected for dry and hot climate regions and within the predicted range for wet and cold climate regions. Regarding CO_2 emissions, when comparing our results with emissions from regions with the same land use, it is important to note that emissions in our study were not controlled (1.40 μmol m^{-2} s^{-1} = 1.45 g m^{-2} day^{-1} of C) and managed (0.97 μmol m^{-2} s^{-1} = 1 g m^{-2} day^{-1}C) pastures (Table 1) were lower than in undegraded temperate regions of South Africa (~1.78 g m^{-2} day^{-1}C) (Abdalla et al., 2018). This difference is largely attributable to the region's climate, feed type, and management.

The spatial correlation of organic groups obtained through FTIR analysis and soil attributes indicated that pH played a significant role in the chemical stability of SOM after pasture renewal (Figs. 6 and 4). During the decomposition of SOM, functional groups are formed that interact with the surrounding environment (Bai et al., 2015). The formation and diversification of functional groups resulting from SOM decomposition, in conjunction with pH, can influence the ionization of organic groups, thereby affecting the chemical stability of SOM (Parolo et al., 2017). Therefore, it is crucial to consider the entire system. In one of the study areas, limestone was applied and incorporated to renew the pasture, followed by the cultivation of forage sorghum, which was later used for silage. These practices significantly altered the intensity and distribution of spectral peaks in the studied pasture systems. While forage sorghum, including *U. brizantha*, has a high carbon-to-nitrogen ratio and does not contribute substantially to straw input due to biomass removal for silage production (Herrera et al., 2020), the spatial variability of compound concentrations in Band A allowed us to infer the quality of the material in both areas. Concentrations of compounds in Band A were spatially correlated with CO_2 emissions, following changes in soil acidity. As well as assisting in the estimates and prediction of emissions in the proposed model.

Liming was a key factor in this study due to its potential effects on the deprotonation of functional groups and alteration of CO_2 fluxes. In addition to the changes caused by SOM functional groups, liming, by improving the chemical conditions of the soil, can lead to increased production of root exudates and often modulate microbial activity, which affects SOM decomposition (Hoffmann et al., 2014; Soussana et al., 2007). Thus, liming has implications for carbon storage and sequestration in the soil. The dynamics of CO_2 fluxes associated with FTIR spectra were consistent with the presence of molecules such as polysaccharides (symmetrical and asymmetrical stretching vibrations of CH bonds, between 2955 and 2835 cm^{-1}). These compounds were effectively influenced by soil pH in the managed pasture system, resulting in reduced CO_2 emissions.

4.1. Main limitations

In this study, we evaluated the impact of degraded pasture renovation on SOM quality and its effect on CO_2 mitigation and emissions using FTIR and statistical spectroscopy. Our assessments were conducted under specific management and climate conditions, without considering organic matter pools or the role of soil microbiota. Given the long-term management regimes of tropical pastures (renovation intervals), we encourage future studies to conduct more targeted experiments that consider the effects of climate change and management practices, such as fertilizer and lime application, rainfall patterns, and grazing intensity. Incorporating these management and climate conditions, along with microbiological and isotopic analyses, will provide deeper insights into the mechanisms governing soil carbon pools and aid in the development of effective CO_2 emission mitigation strategies.

To ensure the sustainable provision of various ecosystem services from tropical pastures, including adequate forage supply for animal feed and minimizing the impact of livestock on CO_2 emissions and global warming, long-term studies are needed to elucidate the influence of climate seasonality (such as warming, drought, and increased precipitation) on ecosystem functioning, carbon storage, and fluxes. The effects of climate change on pastures are still poorly understood, underscoring the need for further research at various scales, employing approaches and methods that link the molecular quality of SOM to greenhouse gas fluxes. This will enhance our understanding of the functions and mechanisms operating in the region and provide valuable insights for informed decision-making.

5. Final remarks

The combination of FTIR spectroscopy and machine learning techniques was sensitive enough to distinguish chemical changes in soil organic groups and predict soil CO_2 emissions in pasture reform systems. The peaks of the organic compounds obtained in the FTIR spectra were spatially dependent and correlated with soil CO_2 emissions and pH.

Soil management practices followed by the cultivation of sorghum intercropped with *U. brizantha* reduced the concentration of labile compounds with spectral signatures in 2923 and 2853 cm^{-1}, and reduced emissions of CO_2 from the soil. We believe that our results can provide a basis for future studies in which the combination of FTIR and machine learning enable large-scale monitoring of SOC composition and possible estimates of carbon loss via CO_2 emission.

Declaration of Competing Interest

The authors declare that they have no known competing financial interests or personal relationships that could have appeared to influence the work reported in this paper.

Data availability

Data will be made available on request.

Appendix A. Supplementary data

Supplementary data to this article can be found online at https://doi.org/10.1016/j.geodrs.2023.e00690.

References

Abdalla, K., Mutema, M., Chivenge, P., Everson, C., Chaplot, V., 2018. Grassland degradation significantly enhances soil CO_2 emission. Catena 167, 284–292. https://doi.org/10.1016/j.catena.2018.05.010.

Allen, D.T., Palen, E.J., Haimov, M.I., Hering, S.V., Young, J.R., 1994. Fourier transform infrared spectroscopy of aerosol collected in a low pressure impactor (LPI/FTIR): method development and field calibration. Aerosol Sci. Technol. 21 (4), 325–342.

Almeida, E.J., Luizão, F., de Rodrigues, D.J., 2015. Litterfall production in intact and selectively logged forests in southern of Amazonia as a function of basal area of vegetation and plant density. Acta Amaz 45, 157–166. https://doi.org/10.1590/1809-4392201402543.

Arantes, V., Milagres, A.M., 2009. Relevance of low molecular weight compounds produced by fungi and involved in wood biodegradation. Quim Nova 32, 1586–1595. https://doi.org/10.1590/S0100-40422009000600043.

Armstrong, R.D., Millar, A.G., Halpin, N.V., Reid, D.J., Standley, J., 2003. Using zero tillage, fertilisers and legume rotations to maintain productivity and soil fertility in opportunity cropping systems on a shallow Vertosol. Aust. J. Exp. Agric. 43, 141–153. https://doi.org/10.1071/EA01175.

Bai, M., Qin, G., Sun, Z., Long, G., 2015. Relationship between molecular structure characteristics of feed proteins and protein in vitro digestibility and solubility. Asian Australas. J. Anim. Sci. 29 (8), 1159–1165. https://doi.org/10.5713/AJAS.15.0701.

Boerjan, W., Ralph, J., Baucher, M., 2003. Lignin biosynthesis. Annu. Rev. Plant Biol. 54, 519–546.

Bruun, T.B., Elberling, B., de Neergaard, A., Magid, J., 2015. Organic carbon dynamics in different soil types after conversion of forest to agriculture. Land Degrad. Dev. 26, 272–283. https://doi.org/10.1002/ldr.2205.

Cambardella, C.A., Moorman, T.B., Novak, J.M., Parkin, T.B., Karlen, D.L., Turco, R.F., Konopka, A.E., 1994. Field-scale variability of soil properties in Central Iowa soils. Soil Sci. Soc. Am. J. 58, 1501–1511. https://doi.org/10.2136/sssaj1994.03615995005800050033x.

Chen, H., Ferrari, C., Angiuli, M., Yao, J., Raspi, C., Bramanti, E., 2010. Qualitative and quantitative analysis of wood samples by Fourier transform infrared spectroscopy and multivariate analysis. Carbohydr. Polym. 82, 772–778. https://doi.org/10.1016/j.carbpol. 2010.05.052.

Cotrufo, M.F., Soong, J.L., Horton, A.J., Campbell, E.E., Haddix, M.L., Wall, D.H., Parton, W.J., 2015. Formation of soil organic matter via biochemical and physical pathways of litter mass loss. Nat. Geosci. 8 (10), 776–779. https://doi.org/10.1038/ngeo2520.

Coates, J., 2000. Interpretation of Infrared Spectra, A Practical Approach. https://doi.org/10.1002/9780470027318.a5606.

de Assis Valadão, F.C., Dos Santos Webe, O.L., Valadao Junior, D.D., Scapinelli, A., Deina, F.R., Bianchini, A., 2015. Adubação fosfatada e compactação do solo: sistema radicular da soja e do milho e atributos físicos do solo. Rev. Bras. Cienc. Solo 39, 243–255. https://doi.org/10.1590/01000683rbcs20150144.

Díaz-Uriarte, R., De Andres, S.A., 2006. Gene selection and classification of microarray data using random forest. BMC Bioinform. 7 (1), 3. https://doi.org/10.1186/1471-2105-7-3.

Duboc, O., Zehetner, F., Djukic, I., Tatzber, M., Berger, T.W., Gerzabek, M.H., 2012. Decomposition of European beech and black pine foliar litter along an alpine elevation gradient: mass loss and molecular characteristics. Geoderma 189, 522–531. https://doi.org/10.1016/j.geoderma.2012.06.018.

Ellert, B.H., Bettany, J.R., 1995. Calculation of organic matter and nutrients stored in soils under contrasting management regimes. Can. J. Soil Sci. 75, 529–538. https://doi.org/10.4141/cjss95-075.

Embrapa, 2017. Manual de métodos de análise de solo.

FAO, 2020. COP26: Agricultural Expansion Drives Almost 90 Percent of Global Deforestation. Available online: https://www.fao.org/newsroom/detail/cop26-agricultural-expansion-drives-almost-90-percent-of-global-deforestation/en. Accessed date: 03 July 2023.

Goydaragh, M.G., Taghizadeh-Mehrjardi, R., Jafarzadeh, A.A., Triantafilis, J., Lado, M., 2021. Using environmental variables and Fourier transform infrared spectroscopy to predict soil organic carbon. Catena 202, 105280. https://doi.org/10.1016/j.catena.2021.105280.

Griffiths, P.R., De Haseth, J.A., 2007. Fourier Transform Infrared Spectrometry. John Wiley & Sons, New York.

Guio Blanco, C.M., Brito Gomez, V.M., Crespo, P., Ließ, M., 2018. Spatial prediction of soil water retention in a Paramo landscape: methodological insight into machine learning using random forest. Geoderma 316, 100–114. https://doi.org/10.1016/j.geoderma.2017.12.002.

Guo, R., Li, G., Jiang, T., Schuchardt, F., Chen, T., Zhao, Y., Shen, Y., 2012. Effect of aeration rate, C/N ratio and moisture content on the stability and maturity of compost. Bioresour. Technol. 112, 171–178. https://doi.org/10.1016/j.biortech.2012.02. 099.

Herrera, A.M., de Mello, A.C.L., Apolinario, V.X.D.O., Dubeux Junior, J.C.B., da Silva, V. J., dos Santos, M.V.F., da Cunha, M.V., 2020. Decomposition of senescent leaves of signalgrass (*Urochloa decumbens* Stapf. R. Webster) and arboreal legumes in silvopastoral systems. Agrofor. Syst. 94, 2213–2224. https://doi.org/10.1007/s10457-020-00542-1.

Herrero, M., Do Valle, C.B., Hughes, N.R.G., De Sabatel, V.O., Jessop, N.S., 2001. Measurements of physical strength and their relationship to the chemical composition of four species of Brachiaria. Anim. Feed Sci. Technol. 92, 149–158. https://doi.org/10.1016/S0377-8401(01)00261-9.

Hoffmann, U., Hoffmann, T., Jurasinski, G., Glatzel, S., Kuhn, N.J., 2014. Assessing the spatial variability of soil organic carbon stocks in an alpine setting (Grindelwald, Swiss Alps). Geoderma 232–234, 270–283. https://doi.org/10.1016/j.geoderma.2014.04.038.

Hurraß, J., Schaumann, G.E., 2006. Properties of soil organic matter and aqueous extracts of actually water repellent and wettable soil samples. Geoderma 132, 222–239. https://doi.org/10.1016/j.geoderma.2005.05.012.

IPCC, 2017. Working Group III (WGIII)-Mitigation of Climate Change Special Report on Climate Change, Desertification, Land Degradation, Sustainable Land Management, Food Security, and Greenhouse Gas Fluxes in Terrestrial Ecosystems (SR2) Background Report for the Scoping Meeting.

José, G.D.A., Cherubin, M.R., Cerri, C.E., Cerri, C.C., Feigl, B.J., 2017. Sugar cane straw left in the field during harvest: decomposition dynamics and composition changes. Soil Res. 55, 758–768. https://doi.org/10.1071/SR16310.

Kögel-Knabner, I., 2002. The macromolecular organic composition of plant and microbial residues as inputs to soil organic matter. Soil Biol. Biochem. 34, 139–162. https://doi.org/10.1016/S0038-0717(01)00158-4.

Lapola, D.M., Martinelli, L.A., Peres, C.A., Ometto, J.P., Ferreira, M.E., Nobre, C.A., Aguiar, A.P., Bustamante, M.M.C., Cardoso, M.F., Costa, M.H., Joly, C.A., Leite, C.C., Moutinho, P., Sampaio, G., Strassburg, B.B.N., Vieira, I.C., 2014. Pervasive transition of the Brazilian land-use system. Nat. Clim. Chang. 4, 27–35. https://doi.org/10.1038/nclimate2056.

Liland, K., 2016. Extended multiplicative signal correction. In: Package "EMSC". Repository CRAN. Available online: https://cran.r-project.org/web/packages/EMSC/index.html.

Liland, K.H., Mevik, B.H., 2015. Baseline: Baseline Correction of Spectra. URL. https://CRAN.R-project.org/package=baseline.

McKee, G.A., Soong, J.L., Calderon, F., Borch, T., Cotrufo, M.F., 2016. An integrated spectroscopic and wet chemical approach to investigate grass litter decomposition chemistry. Biogeochemistry 128, 107–123. https://doi.org/10.1007/s10533-016-0197-5.

Miranda, E., Carmo, J., Couto, E., Camargo, P., 2016. Long-term changes in soil carbon stocks in the Brazilian Cerrado under commercial soybean. Land Degrad. Dev. 27, 1586–1594. https://doi.org/10.1002/ldr.2473.

Mohanty, B., Gupta, A., Das, B.S., 2016. Estimation of weathering indices using spectral reflectance over visible to mid-infrared region. Geoderma 266, 111–119. https://doi.org/10.1016/j.geoderma.2015.11.030.

Nocita, M., Stevens, A., van Wesemael, B., Brown, D.J., Shepherd, K.D., Towett, E., Vargas, R., Montanarella, L., 2015. Soil spectroscopy: an opportunity to be seized. Glob. Chang. Biol. 21, 10–11. https://doi.org/10.1111/gcb.12632.

Parikh, S.J., Goyne, K.W., Margenot, A.J., Mukome, F.N.D., Calderón, F.J., 2014. Soil chemical insights provided through vibrational spectroscopy. In: Sparks, D.L. (Ed.), Advances in Agronomy. Academic Press, New York, pp. 1–148.

Parolo, M.E., Savini, M.C., Loewy, R.M., 2017. Characterization of soil organic matter by FT-IR spectroscopy and its relationship with chlorpyrifos sorption. J. Environ. Manag. 196, 316–322. https://doi.org/10.1016/J.JENVMAN.2017.03.018.

Paul, E.A., 2016. The nature and dynamics of soil organic matter: plant inputs, microbial transformations, and organic matter stabilization. Soil Biol. Biochem. 98, 109–126. https://doi.org/10.1016/j.soilbio.2016.04.001.

Pauly, M., Keegstra, K., 2008. Cell-wall carbohydrates and their modification as a resource for biofuels. Plant J. 54, 559–568. https://doi.org/10.1111/j.1365-313X.2008.03463.x.

Piccolo, A., Zaccheo, P., Genevini, P.G., 1992. Chemical characterization of humic substances extracted from organic-waste-amended soils. Bioresource Technol. 40, 275–282. https://doi.org/10.1016/0960-8524(92)90154-P.

Pimentel, L.G., Barreto, M.S.C., da Silva Oliveira, D.M., Cherubin, M.R., Dematê, J.A.M., Cerri, C.E.P., Cerri, C.C., 2019. Diffuse reflectance infrared Fourier transform (DRIFT) spectroscopy to assess decomposition dynamics of sugarcane straw. Bioenergy Res. 12, 909–919. https://doi.org/10.1007/s12155-019-10024-7.

Qin, Q., Wang, H., Li, X., Xie, Y., Lei, X., Zheng, Y., Yang, D., Wang, F., 2019. Spatial heterogeneity and affecting factors of litter organic carbon and total nitrogen over natural spruce-fir mixed forests in northeastern China. Catena 174, 293–300. https://doi.org/10.1016/j.catena.2018.11.020.

Rask, K.J., Rask, N., 2011. Economic development and food production–consumption balance: a growing global challenge. Food Policy 36, 186–196. https://doi.org/10.1016/j.foodpol.2010.11.015.

Ray, D.K., Mueller, N.D., West, P.C., Foley, J.A., 2013. Yield trends are insufficient to double global crop production by 2050. PLoS One 8, e66428. https://doi.org/10.1371/journal.pone.0066428.

Reitner, J., Quéric, N.V., Arp, G., Mastandrea, A., Guido, A., Demasi, F., Russo, F., 2011. The characterisation of sedimentary organic matter in carbonates with Fourier-transform infrared (FTIR) spectroscopy. In: Advances in Stromatolite Geobiology, pp. 331–342.

Rial, M., Cortizas, A.M., Rodríguez-Lado, L., 2016. Mapping soil organic carbon content using spectroscopic and environmental data: a case study in acidic soils from NW Spain. Sci. Total Environ. 539, 26–35. https://doi.org/10.1016/j.scitotenv.2015.08.088.

Rossel, R.V., Walvoort, D.J.J., McBratney, A.B., Janik, L.J., Skjemstad, J.O., 2006. Visible, near infrared, mid infrared or combined diffuse reflectance spectroscopy for simultaneous assessment of various soil properties. Geoderma 131 (1–2), 59–75. https://doi.org/10.1016/j.geoderma.2005.03.007.

Sanz, M.J., de Vente, J., Chotte, J.L., Bernoux, M., Kust, G., Ruiz, I., Almagro, M., Alloza, J.A., Vallejo, R., Castillo, V., Hebel, A., Akhtar-Schuster, M., 2017. Sustainable Land Management Contribution to Successful Land-Based Climate Change Adaptation and Mitigation. Boon.

Schwartz, R.C., Baumhardt, R.L., Evett, S.R., 2010. Tillage effects on soil water redistribution and bare soil evaporation throughout a season. Soil Tillage Res. 110, 221–229. https://doi.org/10.1016/j.still.2010.07.015.

Schwarz, W., 2001. The cellulosome and cellulose degradation by anaerobic bacteria. Appl. Microbiol. Biotechnol. 56, 634–649. https://doi.org/10.1007/s002530100710.

Senesi, N., Plaza, C., Brunetti, G., Polo, A., 2007. A comparative survey of recent results on humic-like fractions in organic amendments and effects on native soil humic substances. Soil Biol. Biochem. 39, 1244–1262. https://doi.org/10.1016/j.soilbio.2006.12.002.

Silva, E.F., Moitinho, M.R., Teixeira, D.B., Pereira, G.T., La Scala Junior, N., 2014. Emissão de CO2 do solo associada à calagem em área de conversão de laranja para Cana-de-açúcar. Eng. Agric. 34, 885–898. https://doi.org/10.1590/s0100-69162014000500008.

Six, J., Frey, S.D., Thiet, R.K., Batten, K.M., 2006. Bacterial and fungal contributions to carbon sequestration in agroecosystems. Soil Sci. Soc. Am. J. 70, 555–569. https://doi.org/10.2136/sssaj2004.0347.

Soares, M.B., da Freddi, O.S., da Matos, E.S., Tavanti, R.F.R., Wruck, F.J., de Lima, J.P., Marchioro, V., Franchini, J.C., 2020. Integrated production systems: an alternative to soil chemical quality restoration in the Cerrado-Amazon ecotone. Catena 185, 104279. https://doi.org/10.1016/j.catena.2019.104279.

Soil Survey Staff, 2014. Keys to Soil Taxonomy | NRCS, 12th ed. Washington.

Soong, J.L., Calderon, F.J., Betzen, J., Cotrufo, M.F., 2014. Quantification and FTIR characterization of dissolved organic carbon and total dissolved nitrogen leached from litter: a comparison of methods across litter types. Plant Soil 385, 125–137. https://doi.org/10.1007/s11104-014-2232-4.

Soussana, J.F., Allard, V., Pilegaard, K., Ambus, P., Amman, C., Campbell, C., Ceschia, E., Clifton-Brown, J., Czobel, S., Domingues, R., Flechard, C., Fuhrer, J., Hensen, A., Horvath, L., Jones, M., Kasper, G., Martin, C., Nagy, Z., Neftel, A., Raschi, A., Baronti, S., Rees, R.M., Skiba, U., Stefani, P., Manca, G., Sutton, M., Tuba, Z., Valentini, R., 2007. Full accounting of the greenhouse gas (CO_2, N_2O, CH_4) budget of nine European grassland sites. Agric. Ecosyst. Environ. 121, 121–134. https://doi.org/10.1016/j.agee.2006.12.022.

Sposito, G., 1989. The Chemistry of Soils. Oxford University Press, New York, pp. 127–146.

Swift, M.J., Heal, O.W., Anderson, J.M., 1979. Decomposition in Terrestrial Ecosystem. University of California Press, Berkley, California, USA.

Tatzber, M., Stemmer, M., Spiegel, H., Katzlberger, C., Haberhauer, G., Mentler, A., Gerzabek, M.H., 2007. FTIR-spectroscopic characterization of humic acids and humin fractions obtained by advanced NaOH, Na4P2O7, and Na2CO3 extraction procedures. J. Plant Nutr. Soil Sci. 170, 522–529. https://doi.org/10.1002/jpln.200622082.

Tavanti, R.F., Montanari, R., Panosso, A.R., Freddi, O.D.S., Paz-González, A., 2020a. Pedotransfer function to estimate the soil structural "s" index and spatial variability in an oxisol within a livestock farming system. Eng. Agríc. 40, 34–44. https://doi.org/10.1590/1809-4430-Eng.Agric.v40n1p34-44/2020.

Tavanti, R.F.R., Montanari, R., Panosso, A.R., La Scala Jr, N., Neto, M.C., Freddi, O.S., González, A.P., Carvalho, M.A.C., Soares, M.B., Tavanti, T.R., Galindo, F.S., 2020b. What is the impact of pasture reform on organic carbon compartments and CO_2 emissions in the Brazilian Cerrado? Catena 194, 104702. https://doi.org/10.1016/j.catena.2020.104702.

Tilman, D., Cassman, K.G., Matson, P.A., Naylor, R., Polasky, S., 2002. Agricultural sustainability and intensive production practices. Nature 418, 671–677. https://doi.org/10.1038/nature01014.

Tilman, D., Balzer, C., Hill, J., Befort, B.L., 2011. Global food demand and the sustainable intensification of agriculture. Proc. Natl. Acad. Sci. 108, 20260–20264. https://doi.org/10.1073/pnas.1116437108.

Torres, J.L.R., Pereira, M.G., Andrioli, I., Polidoro, J.C., Fabian, A.J., 2005. Decomposição e liberação de nitrogênio de resíduos culturas de plantas de cobertura em um solo de cerrado. Rev. Bras. Cienc. Solo 29, 609–618. https://doi.org/10.1590/s0100- 06832005000400013.

Van Raij, B., de Andrade, J.C., Cantarella, H., Quaggio, J.A., 2001. Análise química para avaliação da fertilidade de solos tropicais, first ed. Instituto Agronômico, Campinas.

Van Soest, P.J., Robertson, J.B., Lewis, B.A., 1991. Methods for dietary fiber, neutral detergent fiber, and nonstarch polysaccharides in relation to animal nutrition. J. Dairy Sci. 74, 3583–3597. https://doi.org/10.3168/jds.S0022-0302(91)78551-2.

Vieira, S.A., Alves, L.F., Aidar, M., Araújo, L.S., Baker, T., Batista, J.L.F., Campos, M.C., Camargo, P.B., Chave, J., Delitti, W.B.C., Higuchi, N., Honorio, E., Joly, C.A., Keller, M., Martinelli, L.A., De Mattos, E.A., Metzker, T., Phillips, O., Dos Santos, F.A. M., Shimabukuro, M.T., Silveira, M., Trumbore, S.E., 2008. Estimation of biomass and carbon stocks: the case of the Atlantic Forest. Biota Neotrop. 8, 21–29. https://doi.org/10.1590/S1676-06032008000200001.

West, T.O., Post, W.M., 2002. Soil organic carbon sequestration rates by tillage and crop rotation. Soil Sci. Soc. Am. J. 66, 1930–1946. https://doi.org/10.2136/sssaj2002.1930.

Wiesmeier, M., Barthold, F., Blank, B., Kogel-Knabner, I., 2011. Digital mapping of soil organic matter stocks using random forest modeling in a semi-arid steppe ecosystem. Plant Soil 340 (1–2), 7–24. https://doi.org/10.1007/s11104-010-0425-z.

Wilks, D.S., 2006. Statistical Methods in the Atmospheric Sciences, Second edition. International Academic Press, p. 627.

Yao, X., Yu, K., Deng, Y., Zeng, Q., Lai, Z., Liu, J., 2019. Spatial distribution of soil organic carbon stocks in Masson pine (*Pinus massoniana*) forests in subtropical China. Catena 178, 189–198. https://doi.org/10.1016/j.catena.2019.03.004.

Yeomans, J.C., Bremner, J.M., 1988. A rapid and precise method for routine determination of organic carbon in soil1. Commun. Soil Sci. Plant Anal. 19, 1467–1476. https://doi.org/10.1080/00103628809368027.